Epitaxial growth of WO_{3-x} needles on (10 $\bar{1}$0) and (01 $\bar{1}$0) WC surfaces produced by controlled oxidation with CO_2

Andrew P. E. York,[a] Jeremy Sloan[a,b] and Malcolm L. H. Green*[a]

[a] *Inorganic Chemistry Laboratory, University of Oxford, South Parks Road, Oxford, UK OX1 3QR. E-mail: malcolm.green@chem.ox.ac.uk*

[b] *Department of Materials, University of Oxford, Parks Road, Oxford, UK OX1 3PH*

Received (in Bath, UK) 23rd September 1998, Accepted 4th January 1999

The controlled oxidation with CO_2 of both high surface area (high S_g) and low surface area WC to form WO_{3-x} needles, has been observed *in situ*, inside a controlled environment transmission electron microscope (CETEM), and also *ex situ*, in a standard flow reactor; the tungsten oxide needles, which consist mainly of distorted γ-$WO_{2.72}$, propagate in an epitaxial fashion from the (10 $\bar{1}$0) and (01 $\bar{1}$0) surfaces of the parent WC crystals; possible mechanisms for the formation of the needles are proposed.

Recently, WC was shown to be an active catalyst for the conversion of methane and carbon dioxide to synthesis gas (CO + H_2).[1,2] During the course of these studies, it was found that catalyst deactivation due to oxidation of WC by CO_2 leads to the formation of tungsten oxides, which are inactive for methane reforming. Such materials are, however, useful in a wide variety of applications including some catalytic processes (*e.g.* metathesis),[3] in optoelectronic devices,[4] as gas sensor materials,[5] and have recently been developed as precursor materials for the synthesis of inorganic fullerene-like (IF) materials based on 2H-WS_2 layered chalcogenide structures.[6–8] While using CETEM to probe the deactivation mechanism of the carbide, we observed the propagation of oxygen deficient tungsten oxide needles from specific crystal faces of the parent carbide. We describe here their *in situ* and *ex situ* formation from both high and low surface area WC particles by controlled oxidation with CO_2.

High surface area (high S_g) WC (40 m^2 g^{-1}) was synthesised by reacting WO_3 with a mixture of 20% CH_4–H_2 (100 ml min^{-1}), ramping the temperature from room temperature to 750 °C at a rate of 1 °C min^{-1}.[2] This material was then characterised by XRD and found to be hexagonal WC with an average particle size radius of 7.62 nm (Scherrer method). The low surface area (low S_g) WC (Alfa Chemicals, 99.5%) exhibited average particle sizes of *ca.* 2.5 μm, estimated by high resolution transmission electron microscopy (HRTEM).

The oxidation of WC in the presence of CO_2 was initially investigated *in situ* in a 400 kV CETEM, described previously.[9,10] Cooling effects due to the thermal conductivity of CO_2 have been taken into account in the reaction temperatures quoted. Both WC samples were heated, under differential pumping conditions, in the temperature range 550–650 °C with an introduced partial pressure of 5 mbar CO_2. The onset of oxidation for high S_g WC was observed at 550–560 °C by formation of WO_{3-x} needles from the surfaces of the WC crystals. For low S_g WC, needle growth started at 580–590 °C, suggesting a slightly higher activation energy for this oxidation. In both cases, needle growth could be observed *in situ* in real time and Fig. 1(a) shows a typical example of growth observed from a cluster of high S_g WC crystallites after *ca.* 20 min at 580 °C. In the case of low S_g (*i.e.* large particle size) WC, parallel multiple needle growth was also observed from the facets of individual WC crystallites. Fig. 1(b) shows six WO_{3-x} needles growing from the (01 $\bar{1}$0) facet of a WC with its [10 $\bar{1}$0] zone axis orientated parallel to the electron beam (SAED not shown). This reaction was subsequently repeated *ex situ* for

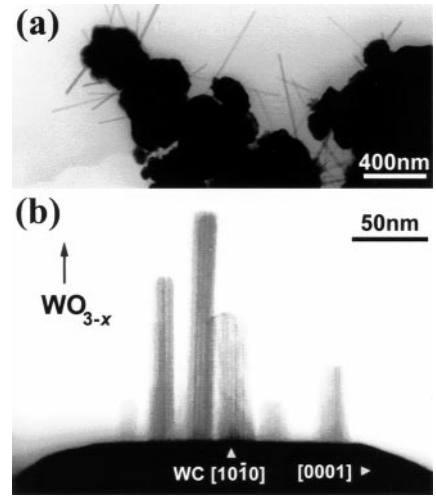

Fig. 1 (a) Micrograph showing WO_{3-x} needle formation from clusters of high S_g WC observed by CETEM. (b) Micrograph showing multiple parallel WO_{3-x} needle growth occurring from the (10 $\bar{1}$0) (alternatively (01 $\bar{1}$0)) face of a single WC crystal in the same [01 $\bar{1}$0] orientation as the example in Fig. 2 (SAED pattern not shown).

both the low and high S_g carbides in a standard flow reactor at ambient pressure and in the temperature range 600–800 °C using a CO_2 flow rate of 100 ml min^{-1} for 24 h. At 750–800 °C, the yield of WO_{3-x} needles from WC from both specimens was quantitative. Partially oxidised WC showing epitaxial needle growth was observed in samples oxidised at 600–750 °C.

For the low S_g WC, it was possible to correlate the WO_{3-x} needle growth with respect to either the (10 $\bar{1}$0) or the (01 $\bar{1}$0) face of the parent carbide; growth from the hexagonal (0001) face was not observed. The middle section of Fig. 2 shows a HRTEM micrograph of the interface between a WO_{3-x} needle grown on the surface of a WC crystallite. The inset indexed SAED pattern **I** (obtained from **I′**) corresponds to a [01 $\bar{1}$0] projection of the parent carbide. The dense microstructure of this crystal is visible below the carbide/oxide interface in the micrograph. Inset **II** is a fast Fourier transform (FFT) computed from region **II′** in the micrograph and shows the calculated diffraction behaviour of the oxide needle. The indicated strong reflections in the centre of **II** correspond to the 0.375 nm layers in the oxide needle. Diffuse streaking in the horizontal rows of diffraction maxima (small arrowheads) correspond to planar disorder occurring parallel to the needle axis (indicated by arrow **A**, micrograph). Substructure reflections, two of which are denoted **A** and **B**, are also visible along these rows. Inset **III**, obtained from the oxide/carbide interface (region **III′**), is an FFT showing the composite diffraction behaviour at the interface. In this pattern, the strong reflections corresponding to the oxide layers are now aligned along [10 $\bar{1}$0] of the WC pattern (large arrow). It is significant that reflection **A** (and its equivalents) from the oxide is now coincident with the WC 0001 reflection (and its equivalents) in **III**, suggesting that the

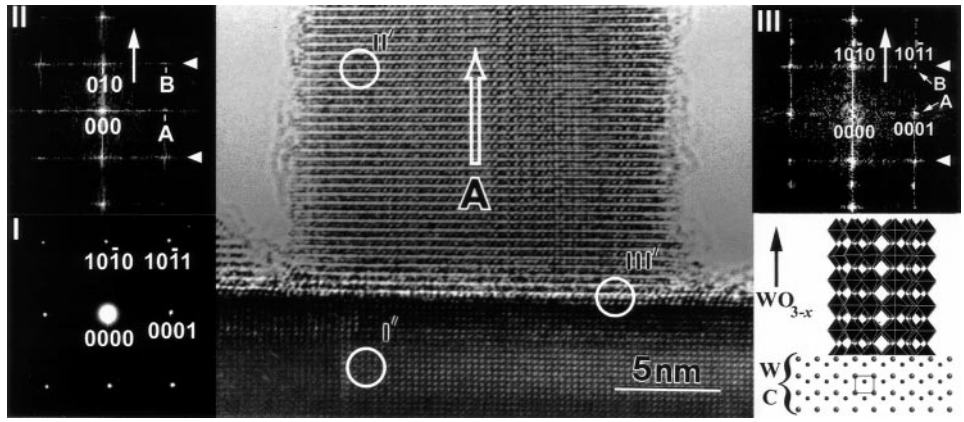

Fig. 2 Micrograph showing the interface between WO_{3-x} needle and WC parent crystal. The inset patterns correspond to: **I**, [01 $\bar{1}$0] SAED pattern obtained from region **I′** corresponding to the parent WC crystal; **II** FFT obtained from region **II′** corresponding to the WO_{3-x} needle; and **III**, FFT obtained from region **III′** corresponding to the WO_{3-x}/WC interface. At the lower right is a schematic representation of the composite microstructure at the interface. The unit cell of the parent carbide (a = 0.2907 nm; c = 0.2837 nm) is indicated.

substructure of the oxide is constrained by that of the carbide, as in a template relationship. This could also be a source of the strain and disorder indicated by the streaking in **II** and **III**. A schematic representation of the overall microstructure is given at the lower right of Fig. 2.

The projection of the oxide in **II** and **III** closely resembles a [001] projection of the phase γ-$WO_{2.72}$ and reflections **A** and **B** (corresponding to 0.284 and 0.220 nm, respectively), are close to (006) and (016) (corresponding to 0.276 and 0.223 nm, respectively) of this oxide.[11,12] Also, the microstructures of the epitaxially grown oxide and γ-$WO_{2.72}$ are very similar as revealed by a comparison of an enlarged region of Fig. 2 [Fig. 3(a)] and an image simulation[13] calculated for a [001] projection of the latter [Fig. 3(b)].

The possible mechanisms for needle formation from the carbides should be addressed. It is proposed that the first step in the formation of the oxide needles is the dissociation of carbon dioxide on the WC surface, according to reaction (1), in agreement with the proposed mechanism for the reforming of methane published by Green and coworkers.[1,2,14] According to this mechanism, oxidation of WC by CO_2 is solely a surface phenomenon and gas-phase dioxygen is not involved.

$$WC + CO_2 = WO_x + CO \quad (1)$$

After the formation of surface oxide, two possible needle propagation mechanisms may be envisaged: (i) an insertion/diffusion mechanism whereby the oxide forms layer-by-layer resulting in platelets that are pushed from below as oxidation diffuses into the carbide crystal; and (ii) a gas-phase reaction involving the transport of oxide from the carbide surface to the oxide needle tips. If mechanism (i) were responsible, progressive consumption of the carbide crystals from the inside should have been observed, but this was not the case.

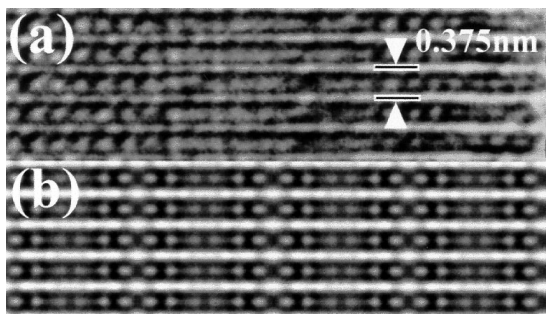

Fig. 3 (a) Enlargement of a segment of the WO_{3-x} needle in Fig. 2. (b) Image simulation calculated for a [001] projection of γ-$WO_{2.72}$ computed using a 1.4 nm thick foil at −70 nm defocus. There is a close (though not perfect) correspondence between the two microstructures.

Mechanism (ii) allows for the epitaxial growth of the needles from the WC crystal surfaces which is apparently observed. Possible support for this is given by the observation of amorphous material on the surface of the needle and the carbide (see Fig. 2) which may correspond to the sublimate feedstock. In addition, the vapour pressure of WO_3 at 550 and 650 °C, and 1 atm (*i.e.* similar conditions to those employed for *ex situ* needle growth) is 5×10^{-4} and 0.0193 mmHg respectively,[15] indicating that tungsten oxide will have a significant presence in the gas-phase. Therefore, we propose that needle growth proceeds *via* mechanism (ii).

The epitaxial growth of orientated WO_{3-x} needles on (10 $\bar{1}$0) and (01 $\bar{1}$0) WC facets by controlled oxidation has been demonstrated. Such a process may, with further development, allow greater control over the stoichiometry and morphology of the produced tungsten oxide needles. We will discuss the issues raised by this work more fully in a future publication.

A. P. E. Y. is grateful to CANMET for financial support; we would also like to thank Ron Doole of the Department of Materials for his assistance with the CETEM.

Notes and references

1 A. P. E. York, J. B. Claridge, A. J. Brungs, S. C. Tsang and M. L. H. Green, *Chem. Commun.*, 1997, 39.
2 A. P. E. York, J. B. Claridge, A. J. Brungs, S. C. Tsang and M. L. H. Green, *Stud. Surf. Sci. Catal.*, 1997, **110**, 711.
3 A. G. Basrur, S. R. Patwardhan and S. N. Vyas, *J. Catal.*, 1991, **127**, 86.
4 S. Passerini, B. Scrosati, V. Hermann, C. Holmblad and T. Bartlett, *J. Electrochem. Soc.*, 1994, **141**, 1025.
5 H. T. Sun, C. Cantalini, L. Lozzi, M. Passacantando, S. Santucci and M. Pelino, *Thin Solid Films*, 1996, **287**, 258.
6 R. Tenne, L. Margulis, M. Genut and G. Hodes, *Nature*, 1993, **360**, 444.
7 L. Margulis, G. Salitra, R. Tenne and M. Talianker, *Nature*, 1993, **365**, 113.
8 M. Homyonfer, B. Alperson, Y. Rosenberg, L. Sapir, S. R. Cohen, G. Hodes and R. Tenne, *J. Am. Chem. Soc.*, 1997, **119**, 2693.
9 R. C. Doole, G. M. Parkinson and J. M. Stead, *Inst. Phys. Conf. Series*, 1991, **119**, 157.
10 R. C. Doole, G. M. Parkinson, J. L. Hutchison, M. J. Goringe and P. J. F. Harris, *JEOL News*, 1992, **30E**, 14.
11 A. Magnéli, *Ark. Kemi*, 1949, **1**, 223.
12 A. Magnéli, Powder Diffraction File card 5-392 (ASTM, Philadelphia Pennsylvania).
13 P. A. Stadelmann, *Ultramicroscopy*, 1987, **21**, 131.
14 J. B. Claridge, A. P. E. York, A. J. Brungs, C. Márquez-Alvarez, J. Sloan, S. C. Tsang and M. L. H. Green, *J. Catal.*, 1998, **180**, 85.
15 *Gmelins Handbuch der Anorganischen Chemie*, ed. R. J. Meyer, Verlag Chemie, Berlin, 1933, vol. 54, p. 122.

Communication 8/07403H